Original Scientific Paper https://doi.org/10.24867/GRID-2026-p74

Development of Green-Synthesized Silver Nanoparticle-Containing PCL Coatings for Paper Packaging Materials

Filiz Kara

Baskent University, Faculty of Engineering, Department of Industrial Engineering, Ankara, Türkiye

ABSTRACT

Growing environmental concerns and the increasing demand for sustainable packaging materials have accelerated the development of biodegradable and functional paper-based packaging systems. Although paper is widely preferred for its excellent printability, low cost, and recyclability, its inherently poor barrier properties limit its use, particularly in food packaging. Surface coating with biodegradable polymers and antimicrobial nanomaterials has emerged as an effective strategy to overcome these limitations while preserving the desirable characteristics of paper. Among antimicrobial nanomaterials, silver nanoparticles (AgNPs) have attracted considerable attention owing to their broad-spectrum antibacterial activity. Green synthesis approaches further enhance their sustainability by eliminating the need for hazardous reducing agents, with hydroxyethly cellulose (HEC) serving as both a reducing and stabilizing agent. In this study, AgNPs synthesized via an HEC-mediated, autoclave-assisted one-pot green synthesis method were incorporated into a polycaprolactone (PCL) matrix and applied onto paper substrates to improve their functional performance. UV–Vis spectroscopy showed a characteristic absorption band at approximately 430 nm, while DLS analysis revealed an average hydrodynamic particle size of 240 nm with a PDI of 0.303. PCL coating formulations containing different amounts of AgNP were applied onto coarse filter paper surfaces in two layers using a glass rod. The structural, thermal, and surface properties of the coated papers were evaluated by ATR-FTIR spectroscopy, thermogravimetric analysis (TGA), water contact angle, and surface free energy measurements. The printability of the coated papers was evaluated using an IGT C1 laboratory printing tester at a printing pressure of 350 N and a printing speed of 1 m min^{-1} using Toyo Process Cyan ink. The color properties of the papers before and after printing were determined using an X-Rite eXact spectrophotometer, while surface gloss was measured using a BYK-Gardner gloss meter. The developed PCL-AgNP coating system successfully combines biodegradability, antimicrobial functionality, and printability while addressing the intrinsic barrier limitations of paper. This environmentally friendly surface modification strategy demonstrates significant potential for developing next-generation active paper-based food packaging materials with enhanced functionality and industrial applicability.

KEY WORDS

Silver nanoparticles, green synthesis, polycaprolactone, paper packaging, antibacterial coating

1. Introduction

Paper-based materials are increasingly considered for packaging applications because they are renewable, recyclable, and biodegradable. However, the porous and hydrophilic nature of cellulose-based paper limits its resistance to moisture, oils, and gases, making uncoated paper unsuitable for many applications that require effective barrier properties. Surface coating is commonly used to overcome these limitations. Although petroleum-based polymers such as polyethylene provide effective protection, their use can reduce the biodegradability and recyclability of paper. This has increased interest in biodegradable polymers as more sustainable coating materials for paper-based packaging (Adak et al., 2025).

Polycaprolactone (PCL) is a biodegradable aliphatic polyester with good film-forming ability and relatively hydrophobic character. These properties make PCL suitable for coating cellulose-based substrates. PCL can also serve as a polymer matrix for incorporating functional agents, making it suitable for the development of active coatings (Lo Faro et al., 2023). The properties of biodegradable polymer coatings can be further modified through the incorporation of nanomaterials. In particular, metal-based nanoparticles can improve the functional performance of these coatings and provide antimicrobial activity, extending their potential use in active packaging systems (Vukoje & Bota, 2025).

Silver nanoparticles (AgNPs) have attracted considerable interest in food packaging due to their strong antimicrobial activity against a broad range of microorganisms. Their high surface-area-to-volume ratio and effectiveness at relatively low concentrations make them suitable for active packaging applications aimed at reducing microbial contamination and extending food shelf life.

AgNPs can be incorporated into polymer matrices, biodegradable films, and surface coatings, making them suitable for the development of functional packaging materials. In addition to providing antimicrobial activity, their incorporation may influence the barrier, thermal, mechanical, and optical properties of the resulting material. For paper-based packaging, AgNP-containing polymer coatings therefore provide a useful approach for combining the advantages of cellulose-based substrates with additional functionality (Okur et al., 2025).

The synthesis method of AgNPs is also important for the development of sustainable functional materials. Conventional chemical synthesis generally requires reducing and stabilizing agents, whereas green synthesis methods aim to simplify nanoparticle production and reduce the use of potentially harmful chemicals. Natural polymers and cellulose derivatives can be useful in this respect because their functional groups can interact with silver ions and with the surface of the resulting nanoparticles.

Hydroxyethyl cellulose (HEC) is a water-soluble, non-ionic cellulose derivative containing abundant hydroxyl groups. HEC has previously been used as a polymeric medium in the preparation of AgNPs and can contribute to nanoparticle formation and stabilization (El-Sheikh et al., 2013) . Its use is therefore suitable for preparing AgNP dispersions that can subsequently be incorporated into polymer-based coating formulations.

Most studies on AgNP-containing papers have focused primarily on antimicrobial or barrier properties. However, adding nanoparticles to a coating can also change the surface and optical characteristics of paper. These changes are important when the coated material is intended to be printed, since color and gloss contribute directly to the appearance of the final product. The amount and distribution of nanoparticles within the coating may affect the original color of the paper as well as its appearance after printing (Todorova et al., 2024; Jung et al., 2018). Evaluating these properties together with wettability and thermal behavior can therefore provide a more complete assessment of AgNP-containing paper coatings.

In this study, AgNPs were prepared by an HEC-mediated, autoclave-assisted one-pot method and subsequently incorporated into PCL coatings applied to coarse filter paper. Three different amounts of the AgNP were used to examine their effect on the coated paper.

The resulting materials were evaluated in terms of chemical structure, thermal behavior, water contact angle, surface free energy, color, and gloss. Color and gloss were also measured after printing with cyan ink to determine how AgNP incorporation affected the appearance of the printed surface.

2. Methods

2.1. Materials

Hydroxyethyl cellulose, polycaprolactone (Sigma-Aldrich), and silver nitrate ($AgNO_3$; ISOLAB Chemicals) were used as raw materials. All solvents and other chemicals used in the experiments were of analytical grade and were used as received without further purification.

2.2. Green Synthesis and Characterization of AgNPs

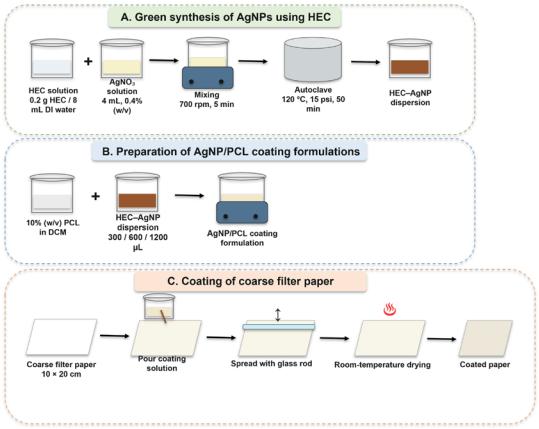
AgNPs were synthesized through a green, one-pot autoclave-assisted method using HEC, without the addition of conventional reducing agents or other toxic chemicals. In this approach, HEC served as the polymeric medium for AgNPs formation under autoclave conditions. First, 0.2 g of HEC was dissolved in 8 mL of deionized water with magnetic stirring.

After complete dissolution, 4 mL of 0.4% (w/v) $AgNO_3$ solution was added slowly, and the mixture was stirred at 700 rpm for 5 min. The solution was then placed in an autoclave (NÜVE NC 90M) and heated at 120 °C and 15 psi for 50 min. A clear change in the color of the solution was observed after autoclaving, providing an initial indication of AgNP formation through the reduction of silver ions (Ag^+) (Figure 1) (Venkatesham et al., 2014). AgNPs formation was examined by UV–Vis spectroscopy over the wavelength range of 200–800 nm using a Hitachi U-1800 spectrophotometer (Digilab, Tokyo, Japan). The hydrodynamic particle size distribution was determined by dynamic light scattering (DLS) using a Zetasizer Nano ZS90 (Malvern Instruments, UK).

2.3. Preparation and Characterization of P-PCL and AgNPs-Loaded Papers

A 10% (w/v) PCL solution was prepared in 10 mL of dichloromethane (DCM) under magnetic stirring. A few drops of Tween 80 were added to facilitate homogeneous dispersion. HEC-AgNP dispersion was then added separately to the PCL solution at volumes of 300, 600, and 1200 µL, and each mixture was thoroughly mixed using a magnetic stirrer. A PCL solution without HEC-AgNPs was prepared in the same manner as the control coating solution. Coarse filter paper (P) (ISOLAB, 60 g/m²) was cut into 10 × 20 cm pieces. The prepared coating solutions were poured onto the paper surfaces and spread uniformly over the entire area. The papers were dried at room temperature, and the coating procedure was repeated to obtain a second layer. After the second application, the coated papers were completely dried at room temperature. The paper coated with PCL alone was designated as P-PCL, whereas the papers coated with PCL containing 300, 600, and 1200 µL of HEC-AgNP dispersion were designated as P-PCL-AgNP1, P-PCL-AgNP2, and P-PCL-AgNP3, respectively (Figure 1).

The chemical structure of the uncoated and coated papers was analyzed by ATR-FTIR spectroscopy using a Thermo Nicolet iS10 spectrometer (Thermo Fisher Scientific, USA). The spectra were recorded over the range of 4000–600 cm^{-1} with 32 scans at a resolution of 4 cm^{-1}. The thermal behavior of the coated papers was evaluated using a TGA 4000 thermogravimetric analyzer (PerkinElmer, USA). The samples were heated from 30 to 750 °C at a heating rate of 10 °C/min under a nitrogen atmosphere. The water contact angles of the coated paper samples were measured using a Pocket Goniometer PG-X, Version 3.4 (FIBRO Systems AB, Sweden). A droplet of deionized water was placed on the coated paper surface, and the droplet profile was recorded using a CCD video camera. The water contact angle was determined from the recorded droplet images. The surface free energy of the coated paper was subsequently calculated based on the measured water contact angle in accordance with ASTM D5946.



» **Figure 1:** *Schematic representation of AgNP synthesis, preparation of coating formulations, and coating of coarse filter paper*

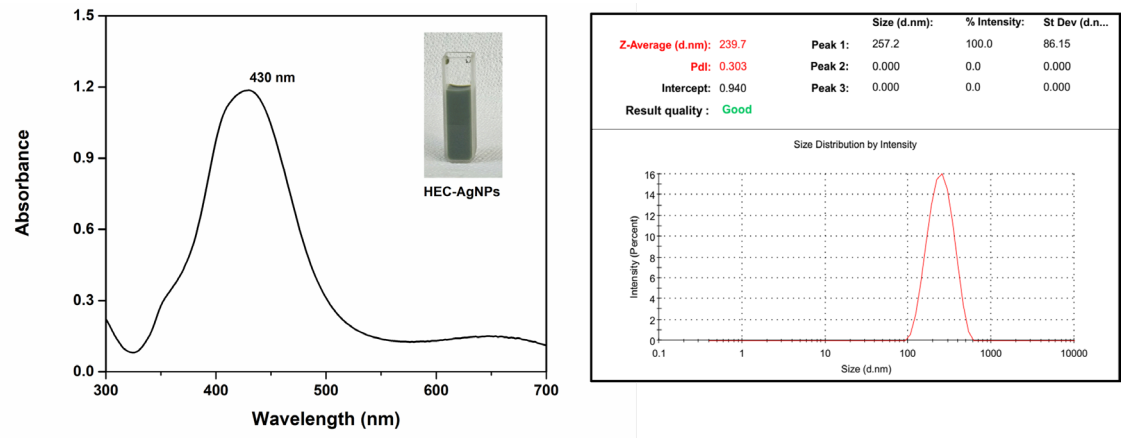
2.4. Printability, Color, and Gloss Measurements

The printability of the coated paper samples was evaluated using an IGTC1 laboratory printing tester. Test prints were produced using Toyo Process Cyan ink under controlled printing conditions. The printing speed was set at 1 m/min, while the applied printing pressure was 350 N. The same printing conditions were used for all coated paper samples to ensure a consistent comparison of their printing performance. The colors of the coated papers before and after printing were measured using an X-Rite eXact portable spectrophotometer in accordance with ISO 13655:2017. Color measurements were performed using a 0°/45° geometry, a 2° standard observer, and a D50 illuminant over the wavelength range of 400–700 nm. The color coordinates were expressed in the CIELAB color space as L*, a*, and b*, where L* represents lightness, a* represents the red–green chromatic coordinate, and b* represents the yellow–blue chromatic coordinate. The gloss of the coated paper surfaces before and after printing was measured using a BYK-Gardner gloss meter according to ISO 8254-1:2009. Gloss measurements were reported in gloss units (GU) using the specified measurement geometry.

3. Results

3.1. UV–Vis and DLS Analysis

The formation of AgNPs was evaluated by UV–Vis spectroscopy. The initially colorless HEC solution changed to dark brown after the reaction, and the corresponding UV–Vis spectrum showed a distinct absorption band centered at approximately 430 nm. DLS measurements showed an average hydrodynamic particle size of 239.7 nm with a PDI value of 0.303 (Figure 2).



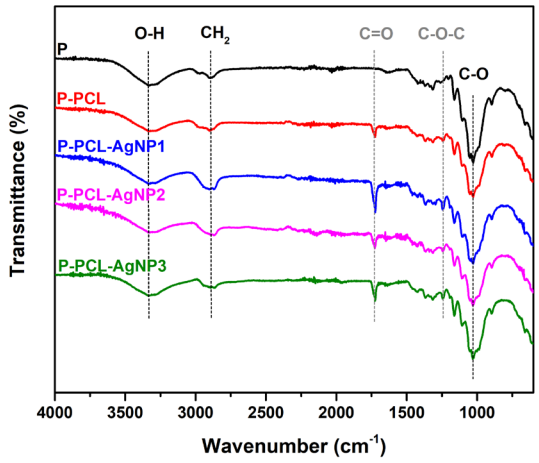
(a) (b)

» **Figure 2:** *(a) UV–Vis absorption spectrum and (b) DLS particle size distribution of HEC-AgNPs*

3.2. ATR-FTIR Analysis

The ATR-FTIR spectra of the uncoated paper (P), PCL-coated paper (P-PCL), and AgNP-containing coated papers (P-PCL-AgNP1, P-PCL-AgNP2, and P-PCL-AgNP3) are shown in Figure 3. The spectrum of P showed a broad band at 3338 cm^{-1} and a C–H stretching band at 2902 cm^{-1}. A weak band was observed at 1647 cm^{-1}. Several bands were also present at 1421, 1371, and 1313 cm^{-1}. Strong absorption bands were observed at 1161 and 1028 cm^{-1}, together with a band at 896 cm^{-1}.

After PCL coating, a new carbonyl band appeared at 1723 cm^{-1} and a band was observed at 1242 cm^{-1}. The carbonyl band was also present in the AgNP-containing samples at 1723, 1728, and 1725 cm^{-1} for P-PCL-AgNP1, P-PCL-AgNP2, and P-PCL-AgNP3, respectively. The band around 1240 cm^{-1} was observed at 1243 cm^{-1} for P-PCL-AgNP1 and 1244 cm^{-1} for P-PCL-AgNP2 and P-PCL-AgNP3. The cellulose bands at around 1161–1163, 1028–1031, and 895–896 cm^{-1} were retained in all coated samples. No new bands or consistent shifts in the main band positions were observed after the addition of HEC-AgNPs.



» **Figure 3:** *FTIR spectra of uncoated and coated papers*

3.3. TGA-DTG Analysis

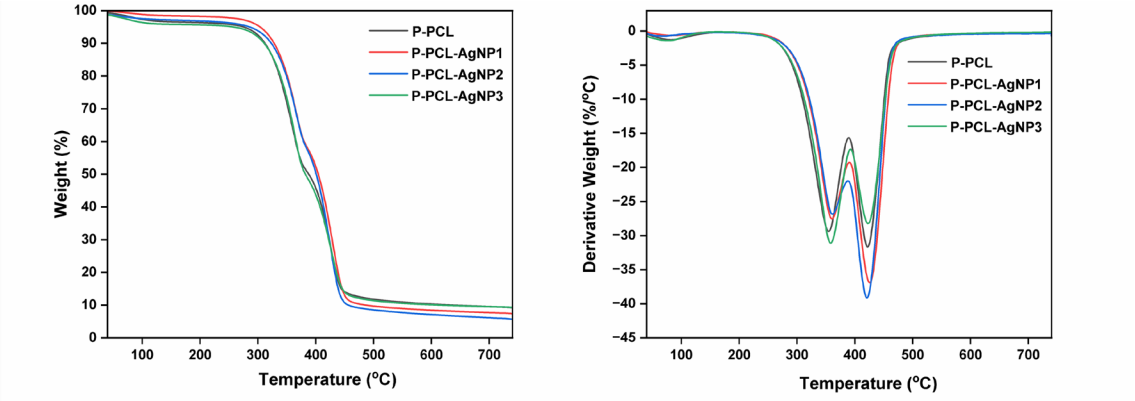
The thermal behavior of P-PCL and AgNP-containing coated papers prepared using AgNPs synthesized in the presence of HEC (P-PCL-AgNP1, P-PCL-AgNP2, and P-PCL-AgNP3) was investigated by TGA and DTG (Figure 4a and 4b). The mass loss below 150 °C was 3.4% for P-PCL, 1.6% for P-PCL-AgNP1, 2.9% for P-PCL-AgNP2, and 4.2% for P-PCL-AgNP3. The main mass loss occurred between approximately 250 and 500 °C.

In this region, two partially overlapping peaks were observed in the DTG curves. The first DTG peak was recorded at 354.7 °C for P-PCL, 360.6 °C for P-PCL-AgNP1, 361.2 °C for P-PCL-AgNP2, and 357.9 °C for P-PCL-AgNP3. The second DTG peak occurred at 421.7, 425.7, 420.7, and 422.8 °C, respectively. The second DTG peak was more pronounced for P-PCL-AgNP1 and P-PCL-AgNP2 than for P-PCL and P-PCL-AgNP3. At 740 °C, the remaining residues were 9.2% for P-PCL, 7.4% for P-PCL-AgNP1, 5.6% for P-PCL-AgNP2, and 9.3% for P-PCL-AgNP3.

3.4. Hydrophilicity and Surface Free Energy

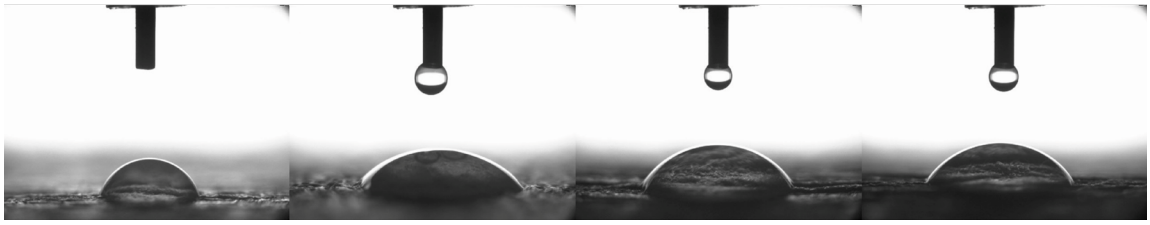
Representative water droplet images of the coated paper samples are shown in Figure 5, while the water contact angle and surface free energy values of all samples, including the uncoated paper, are presented in Table 1. The uncoated paper (P) had a water contact angle of 18.0°, which increased to 72.0° after PCL coating. The addition of AgNPs decreased the contact angle to 49.5°, 48.4°, and 47.9° for P-PCL-AgNP1, P-PCL-AgNP2, and P-PCL-AgNP3, respectively.

The surface free energy showed an opposite trend. The value decreased from 58.6 mJ/m^2 for P to 39.0 mJ/m^2 for P-PCL and then increased to 47.2–47.7 mJ/m^2 after AgNP incorporation. Only small differences were observed among the AgNP-containing samples.



(a) (b)

» **Figure 4:** *TGA (a) and DTG (b) curves of coated papers*



(a) (b) (c) (d)

» **Figure 5:** *Representative water droplet images of (a) P-PCL, (b) P-PCL-AgNP1, (c) P-PCL-AgNP2, and (d) P-PCL-AgNP3*

Table 1
Water contact angle and surface free energy of uncoated and coated papers

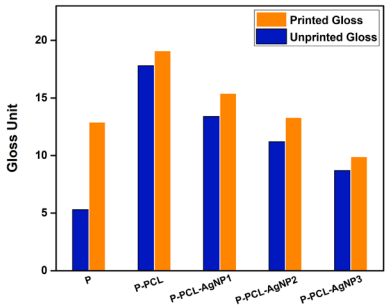
Sample	Water contact angle (°)	Surface free energy (mJ/m²)
P	18.0	58.6
P-PCL	72.0	39.0
P-PCL-AgNP1	49.5	47.2
P-PCL-AgNP2	48.4	47.6
P-PCL-AgNP3	47.9	47.7

3.5. Color and Gloss Measurements

The CIELAB color coordinates of the unprinted and printed paper samples are presented in Table 2. Before printing, P showed L*, a*, and b* values of 89.43, 1.04, and 4.03, respectively. After PCL coating, these values were 91.52, 0.05, and 3.42, respectively. AgNP incorporation resulted in L* values of 89.28, 88.02, and 79.86 for P-PCL-AgNP1, P-PCL-AgNP2, and P-PCL-AgNP3, respectively. The corresponding a* values remained close to zero (0.03, 0.41, and −0.67), whereas the b* values increased progressively from 13.35 to 14.39 and 16.65. After printing with cyan ink, the L* values were 35.41 for P and 31.84 for P-PCL, while values of 38.01, 29.35, and 35.91 were obtained for P-PCL-AgNP1, P-PCL-AgNP2, and P-PCL-AgNP3, respectively.

All printed samples showed negative a* and b* values. The b* value of P-PCL was −50.83 and became progressively less negative with AgNP incorporation, reaching −41.23, −38.72, and −31.07 for P-PCL-AgNP1, P-PCL-AgNP2, and P-PCL-AgNP3, respectively.

The gloss values of the unprinted and printed paper samples are shown in Figure 6. Before printing, the gloss value increased from 5.3 GU for P to 17.8 GU for P-PCL. The AgNP-containing samples showed gloss values of 13.4, 11.2, and 8.7 GU for P-PCL-AgNP1, P-PCL-AgNP2, and P-PCL-AgNP3, respectively. After printing, the gloss value of P-PCL was 19.1 GU, while values of 15.4, 13.3, and 9.9 GU were obtained for P-PCL-AgNP1, P-PCL-AgNP2, and P-PCL-AgNP3, respectively. The decreasing trend in gloss with increasing AgNP addition was maintained after printing.



» **Figure 6:** *Gloss values of the unprinted and printed paper samples*

Table 2
CIELAB color coordinates of the unprinted and printed paper samples

Sample	Before printing L*	a*	b*	After printing L*	a*	b*
P	89.43	1.04	4.03	35.41	−11.64	−49.20
P-PCL	91.52	0.05	3.42	31.84	−7.85	−50.83
P-PCL-AgNP1	89.28	0.03	13.35	38.01	−13.05	−41.23
P-PCL-AgNP2	88.02	0.41	14.39	29.35	−12.81	−38.72
P-PCL-AgNP3	79.86	−0.67	16.65	35.91	−11.48	−31.07

4. Discussion

The color change from colorless to dark brown and the appearance of an absorption band at approximately 430 nm indicate the formation of AgNPs. The absorption band is attributed to the surface plasmon resonance (SPR) of AgNPs, which is generally observed in the 400–500 nm region and is associated with the reduction of Ag^+ ions and formation of metallic silver nanoparticles (Ashraf et al., 2016). SPR bands within approximately 410–450 nm has also been commonly reported for spherical AgNPs (Zaheer & Rafiuddin, 2012). DLS analysis showed an average hydrodynamic particle size of 239.7 nm with a PDI of 0.303. Since DLS measures the hydrodynamic diameter of particles in dispersion, the measured size includes the nanoparticle together with its associated surface layer and surrounding solvated components. The PDI value indicates a moderately polydisperse particle population rather than a highly uniform size distribution (Wang & Wei, 2022).

The FTIR spectrum of the uncoated paper showed the characteristic bands of cellulose (Figure 3). The broad band at 3338 cm^{-1} is assigned to O–H stretching, while the band at 2902 cm^{-1} is related to C–H stretching. The weak band at 1647 cm^{-1} can be associated with adsorbed water in the cellulose structure. The bands at 1421 and 1371 cm^{-1} are related to CH_2 scissoring and C–H bending vibrations, respectively. The band at 1161 cm^{-1} is assigned to asymmetric C–O–C stretching of the glycosidic linkage, while the band at 1028 cm^{-1} is related to C–O stretching of the pyranose ring. The band at 896 cm^{-1} is characteristic of the β-glycosidic linkages of cellulose (Oh et al., 2005).

The main change after PCL coating was the appearance of a strong band at 1723 cm^{-1}, assigned to ester C=O stretching of PCL, together with a band at 1242 cm^{-1} associated with asymmetric ester C–O–C stretching (Elzein et al., 2004). These bands were also observed in all AgNP-containing samples, indicating the presence of PCL in the coated papers. The cellulose bands around 1160, 1030, and 896 cm^{-1} remained visible after coating. HEC is a cellulose ether, and its main FTIR bands overlap with those of the cellulose-based paper (Refaat et al., 2023). Therefore, HEC cannot be clearly distinguished from the paper substrate in the spectra.

The addition of HEC-AgNPs did not produce new bands or consistent shifts in the main PCL and cellulose bands. Small differences were observed mainly in band intensities at 1723 cm^{-1}. These differences may be related to variations in the amount and distribution of the coating within the analyzed area. Overall, the FTIR results showed that the characteristic PCL and cellulose bands were retained after HEC-AgNP incorporation.

The TGA/DTG profiles of all samples showed a similar multi-step degradation pattern, which can be related to the presence of the cellulose-based paper substrate together with HEC and PCL. AgNP incorporation did not substantially alter the overall shape of the degradation profile, although some differences were observed in the degradation temperatures and DTG peak intensities. The mass loss below 150 °C can mainly be attributed to the removal of adsorbed and hydrogen-bonded water.

The hydrophilic hydroxyl groups of cellulose ethers contribute to water retention within the structure, and a similar low-temperature mass loss associated with retained moisture has been observed in HEC-based materials (Zor et al., 2024) . The lower mass loss of P-PCL-AgNP1 and P-PCL-AgNP2 compared with P-PCL may be related to interactions between AgNPs and hydroxyl groups in the polymer chains, which can affect water retention within the structure (Orsuwan, 2023).

In contrast, P-PCL-AgNP3 showed a higher mass loss in this region. This difference may be associated with variations in sample composition and the number of hydrophilic groups available for interaction with water. The first DTG peak appeared between 355 and 361 °C, which falls within the main thermal degradation range of cellulosic materials. Cellulose degradation generally occurs between approximately 315 and 400 °C and involves cleavage of glycosidic bonds and breakdown of the polymer chains (Yang et al., 2007). Therefore, the first DTG peak can be mainly associated with the degradation of the cellulose-based paper substrate and HEC. Compared with P-PCL, which showed this peak at 355 °C, the peak shifted to 361 °C for both P-PCL-AgNP1 and P-PCL-AgNP2 and to 358 °C for P-PCL-AgNP3. These small shifts to higher temperatures may result from interactions between AgNPs and the surrounding polymeric structure.

The effect of AgNPs on thermal degradation can vary depending on the polymer matrix and nanoparticle–polymer interactions, and changes in degradation temperature (Ramos et al., 2014; Orsuwan, 2023). The second DTG peak, observed between 421 and 426 °C, can be mainly associated with PCL degradation. The thermal degradation of PCL involves random chain scission followed by successive depolymerization from the chain ends, with ε-caprolactone formed during the degradation process (Persenaire et al., 2001).

The second peak occurred at 422 °C for P-PCL and at 426, 421, and 423 °C for P-PCL-AgNP1, P-PCL-AgNP2, and P-PCL-AgNP3, respectively. Since the peak temperature did not show a consistent increase after AgNP incorporation, AgNPs had no clear systematic effect on the degradation temperature of PCL. The more pronounced second DTG peak for P-PCL-AgNP1 and P-PCL-AgNP2 indicates a higher degradation rate in this temperature region. This difference may be related to the coating composition and the distribution of AgNPs within the polymer matrix. The residue remaining at 740 °C ranged from approximately 6% to 9% and did not show a consistent change with AgNPs incorporation. The final residue may include carbonaceous products formed during the degradation of the cellulose-based components together with thermally stable silver-containing material (Ramos et al., 2014).

The differences among the samples may therefore result from both the coating composition and the amount of carbonaceous residue formed during thermal degradation. Overall, AgNP incorporation did not change the main multi-step degradation profile of the coated papers. The first DTG peak shifted slightly toward higher temperatures, whereas no consistent change was observed in the second peak associated mainly with PCL degradation. These results suggest that AgNP incorporation caused only minor changes in the thermal degradation behavior of the coated papers without markedly affecting their overall thermal profile.

The uncoated paper (P) showed a low water contact angle (18.0°), which can be related to the hydrophilic hydroxyl groups of cellulose and the porous structure of the paper. After PCL coating, the contact angle increased to 72.0° for P-PCL, showing the lower wettability of the PCL-coated surface. This increase is consistent with the relatively hydrophobic character of PCL. However, the contact angle remained below 90°, which is generally associated with hydrophilic wetting behavior (Law, 2014). AgNP incorporation decreased the water contact angle to 49.5°, 48.4°, and 47.9° for P-PCL-AgNP1, P-PCL-AgNP2, and P-PCL-AgNP3, respectively. The lower contact angles indicate improved wettability of the AgNP-containing coated surfaces compared with P-PCL. This change may be associated with the modification of the surface characteristics after AgNP incorporation.

Since the AgNPs were incorporated as an HEC-based dispersion, the hydroxyl-rich structure of HEC may also contribute to the increased interaction of the coated surface with water (Bellen et al., 2023). Only small differences in contact angle were observed among the three AgNP-containing samples. The surface free energy results followed the opposite trend to the water contact angle. PCL coating decreased the surface free energy from 58.6 mJ/m² for P to 39.0 mJ/m² for P-PCL. After AgNP incorporation, the values increased to 47.2, 47.6, and 47.7 mJ/m² for P-PCL-AgNP1, P-PCL-AgNP2, and P-PCL-AgNP3, respectively. The increase in surface free energy, together with the decrease in water contact angle, indicates improved wettability of the AgNP-containing coated papers.

The incorporation of AgNPs affected the optical appearance of the PCL-coated paper. While the uncoated paper exhibited a relatively neutral appearance, AgNP incorporation resulted in a progressive increase in positive b* values, indicating a gradual shift toward yellowish tones (P-PCL-AgNP3, b* = 16.65). This concentration-dependent optical change can be associated with the presence of AgNPs within the coating layer. The incorporation of AgNPs can affect the optical characteristics of coated paper, and the resulting changes may depend on the amount and distribution of nanoparticles within the coating (Todorova et al., 2024; Jung et al., 2018). The increase in yellowness was accompanied by a decrease in L* at the highest AgNP addition (P-PCL-AgNP3, L* = 79.86). Thus, the highest AgNP formulation produced the most pronounced yellowish and darker appearance among the investigated coatings. This behavior can be attributed to the optical contribution of the AgNP-containing layer. However, AgNP concentration alone may not determine the final color, since particle size, aggregation state, dispersion, and coating structure can also influence the optical response of nanoparticle-containing films and coatings.

Therefore, the observed color changes can be interpreted as a concentration-dependent optical response of the PCL–AgNP coating. The effect of AgNP incorporation was also evident in the surface gloss. PCL application increased the gloss compared with the uncoated paper (17.8 vs. 5.3 GU). However, increasing AgNP addition progressively reduced the gloss, with the lowest value obtained for P-PCL-AgNP3 (8.7 GU). The gloss of nanoparticle-coated paper surfaces is closely related to surface topography, as changes in the coating structure can influence specular reflection (Samyn et al., 2016). Accordingly, the reduction in gloss with increasing AgNP addition may be associated with changes in the surface structure and light-scattering characteristics of the PCL coating. The same concentration-dependent tendency was retained after printing. Although the cyan printing ink dominated the absolute color coordinates, the progressive increase in b* from P-PCL (−50.83) to P-PCL-AgNP1 (−41.23), P-PCL-AgNP2 (−38.72), and P-PCL-AgNP3

(−31.07) indicates that increasing AgNP addition shifted the printed surface toward less negative b* values. In other words, the printed samples became progressively less blue as the AgNP addition increased. This indicates that the optical characteristics of the underlying functional coating were still reflected in the final printed appearance, despite the strong contribution of the cyan ink. The post-print gloss values showed a similar trend. P-PCL exhibited the highest gloss value (19.1 GU), whereas the gloss decreased with increasing AgNP addition, reaching the lowest value for P-PCL-AgNP3 (9.9 GU).

The retention of the same decreasing tendency after printing suggests that the reduction in surface gloss originated primarily from the coated substrate rather than from the printing step itself. Differences in the surface structure and optical roughness of nanoparticle-containing paper coatings can influence their gloss characteristics (Samyn et al., 2011). Overall, the results demonstrate a concentration-dependent effect of AgNP incorporation on both color and gloss. Increasing AgNP addition produced progressively more yellowish coating surfaces while reducing gloss. After printing, the cyan ink became the dominant contributor to the measured color coordinates; nevertheless, the systematic shift toward less negative b* values with increasing AgNP addition indicates that the underlying functional coating continued to influence the final printed appearance. These findings are particularly relevant for active packaging papers, where AgNP addition should be considered not only in relation to functional performance but also to the optical characteristics and print appearance of the final substrate.

5. Conclusions

HEC-mediated AgNPs were successfully incorporated into PCL coatings and applied to coarse filter paper. The addition of AgNPs did not alter the main chemical structure or thermal degradation profile of the PCL-coated papers, but it affected their surface and optical properties. Compared with PCL alone, the AgNP-containing coatings showed lower water contact angles and higher surface free energy, indicating improved surface wettability. Increasing AgNP addition also resulted in a more yellowish appearance and a gradual decrease in surface gloss.

The effect of the coating composition remained visible after printing. Although cyan ink dominated the color of the printed samples, differences associated with AgNP addition were still observed, particularly in the b* values and gloss. Overall, the results show that AgNPs can be incorporated into PCL-coated paper while maintaining the main structural and thermal characteristics of the coating. At the same time, the changes in wettability, color, and gloss indicate that the amount of AgNPs should be considered when such coatings are intended for printed paper-based applications.

6. Acknowledgments

The author thanks Assoc. Prof. Dr. Emine Arman Kandırmaz for her assistance with the color and gloss measurements.

7. References

Adak, B., Baidya, S. and Teramoto, Y. (2025) 'Biopolymers and their nanocomposites coated paper-based high barrier and sustainable food packaging materials', *Carbohydrate Polymers*, 367, 123966. DOI: 10.1016/j.carbpol.2025.123966

Ashraf, J.M., Ansari, M.A., Khan, H.M., Alzohairy, M.A. and Choi, I. (2016) 'Green synthesis of silver nanoparticles and characterization of their inhibitory effects on AGEs formation using biophysical techniques', *Scientific Reports*, 6, 20414. DOI: 10.1038/srep20414

Bellen, F., Carbone, E., Baatsen, P., Jones, E.A.V., Kabirian, F. and Heying, R. (2023) 'Improvement of endothelial cell-polycaprolactone interaction through surface modification via aminolysis, hydrolysis, and a combined approach', *Journal of Tissue Engineering and Regenerative Medicine*, 2023, 5590725. DOI: 10.1155/2023/5590725

El-Sheikh, M.A., El-Rafie, S.M., Abdel-Halim, E.S. and El-Rafie, M.H. (2013) 'Green synthesis of hydroxyethyl cellulose-stabilized silver nanoparticles', *Journal of Polymers*, 2013, 650837. DOI: 10.1155/2013/650837

Elzein, T., Nasser-Eddine, M., Delaite, C., Bistac, S. and Dumas, P. (2004) 'FTIR study of polycaprolactone chain organization at interfaces', *Journal of Colloid and Interface Science*, 273(2), pp. 381–387. DOI: 10.1016/j.jcis.2004.02.001

Jung, J., Raghavendra, G.M., Kim, D. and Seo, J. (2018) 'One-step synthesis of starch-silver nanoparticle solution and its application to antibacterial paper coating', *International Journal of Biological Macromolecules*, 107, pp. 2285–2290. DOI: 10.1016/j.ijbiomac.2017.10.108

Law, K.Y. (2014) 'Definitions for hydrophilicity, hydrophobicity, and superhydrophobicity: Getting the basics right', *The Journal of Physical Chemistry Letters*, 5(4), pp. 686–688. DOI: 10.1021/jz402762h

Lo Faro, E., Bonofiglio, A., Barbi, S., Montorsi, M. and Fava, P. (2023) 'Polycaprolactone/starch/agar coatings for food-packaging paper: Statistical correlation of the formulations' effect on diffusion, grease resistance, and mechanical properties', *Polymers*, 15(19), 3921. DOI: 10.3390/polym15193921

Oh, S.Y., Yoo, D.I., Shin, Y., Kim, H.C., Kim, Y.H., Chung, Y.S., Park, W.H. and Youk, J.H. (2005) 'Crystalline structure analysis of cellulose treated with sodium hydroxide and carbon dioxide by means of X-ray diffraction and FTIR spectroscopy', *Carbohydrate Research*, 340(15), pp. 2376–2391. DOI: 10.1016/j.carres.2005.08.007

Okur, E.E., Eker, F., Akdaşçi, E., Bechelany, M. and Karav, S. (2025) 'Comprehensive review of silver nanoparticles in food packaging applications', *International Journal of Molecular Sciences*, 26(20), 9842. DOI: 10.3390/ijms26209842

Orsuwan, A. (2023) 'Effect of cellulose nanocrystals and green synthesized silver nanoparticles on mechanical properties and antimicrobial activity of banana flour/agar composite films', *Heliyon*, 9(4), e15102. DOI: 10.1016/j.heliyon.2023.e15102

Persenaire, O., Alexandre, M., Degée, P. and Dubois, P. (2001) 'Mechanisms and kinetics of thermal degradation of poly(ε-caprolactone)', *Biomacromolecules*, 2(1), pp. 288–294. DOI: 10.1021/bm0056310

Ramos, M., Fortunati, E., Peltzer, M., Dominici, F., Jiménez, A., Garrigós, M.C. and Kenny, J.M. (2014) 'Influence of thymol and silver nanoparticles on the degradation of poly(lactic acid) based nanocomposites: Thermal and morphological properties', *Polymer Degradation and Stability*, 108, pp. 158–165. DOI: 10.1016/j.polymdegradstab.2014.02.011

Refaat, A., Elhaes, H. and Ibrahim, M.A. (2023) 'Effect of alkali metals on physical and spectroscopic properties of cellulose', *Scientific Reports*, 13, 21649. DOI: 10.1038/s41598-023-48850-7

Samyn, P., Van Erps, J., Thienpont, H. and Schoukens, G. (2011) 'Paper coatings with multi-scale roughness evaluated at different sampling sizes', *Applied Surface Science*, 257(13), pp. 5613–5625. DOI: 10.1016/j.apsusc.2011.01.059

Todorova, D., Yavorov, N. and Vrabič-Brodnjak, U. (2024) 'Impact of silver nanoparticle treatment and chitosan on packaging paper's barrier effectiveness', *Polymers*, 16(15), 2127. DOI: 10.3390/polym16152127

Venkatesham, M., Ayodhya, D., Madhusudhan, A., Babu, N.V. and Veerabhadram, G. (2014) 'A novel green one-step synthesis of silver nanoparticles using chitosan: Catalytic activity and antimicrobial studies', *Applied Nanoscience*, 4(1), pp. 113–119. DOI: 10.1007/s13204-012-0180-y

Vukoje, M. and Bota, J. (2025) 'Effect of PCL nanocomposite coatings on the recyclability of paperboard packaging', *Recycling*, 10(2), 53. DOI: 10.3390/recycling10020053

Wang, Y. and Wei, S. (2022) 'Green fabrication of bioactive silver nanoparticles using Mentha pulegium extract under alkaline: An enhanced anticancer activity', *ACS Omega*, 7(1), pp. 1494–1504. DOI: 10.1021/acsomega.1c06267

Yang, H., Yan, R., Chen, H., Lee, D.H. and Zheng, C. (2007) 'Characteristics of hemicellulose, cellulose and lignin pyrolysis', *Fuel*, 86(12–13), pp. 1781–1788. DOI: 10.1016/j.fuel.2006.12.013

Zaheer, Z. and Rafiuddin (2012) 'Silver nanoparticles to self-assembled films: Green synthesis and characterization', *Colloids and Surfaces B: Biointerfaces*, 90, pp. 48–52. DOI: 10.1016/j.colsurfb.2011.09.037

Zor, M., Yazici, H., Şen, F., Eroğlu, E., Candan, Z., Rodrigue, D. and Wang, X. (2024) 'Preparation and characterization of hydroxyethyl cellulose/nanolignin composite films', *BioResources*, 19(4), pp. 7354–7365. DOI: 10.15376/biores.19.4.7354-7365



© 2026 Authors. Published by the University of Novi Sad, Faculty of Technical Sciences, Department of Graphic Engineering and Design. This article is an open access article distributed under the terms and conditions of the Creative Commons Attribution license 4.0 Serbia (http://creativecommons.org/licenses/by/4.0/rs/).